ISBN: 978-3-95450-204-2 ISSN: 2673-5350 doi:10.18429/JACoW-IBIC2019-WEPP040

OPTIMIZATION OF ANTIPROTON CAPTURE FOR ANTIHYDROGEN CREATION IN THE ALPHA EXPERIMENT

S. Fabbri*, W. Bertsche, University of Manchester, Manchester, England

Abstract

At the ALPHA Experiment at CERN, thin foils of material are used to slow down and trap antiprotons in a Penning trap, where they can be used for antihydrogen creation and measurements. Historically, over 99% of antiprotons are lost during the capture process as a result of the 5.3 MeV initial kinetic energy of the beam delivered by the Antiproton Decelerator. This places a limit early on in the achievable number of antihydrogen. ELENA is a new storage ring coming online which will lower this initial kinetic energy of the beam to 100 keV, improving this efficiency but requiring experiments to update their infrastructure. We present Monte Carlo and particle tracking simulation results for the optimization of the new degrading foil material, thickness, and location in the ALPHA catching Penning trap. From these results, we expect an upper capture efficiency of approximately 50%.

INTRODUCTION

As charged particles pass through a degrader, they are slowed down through inelastic collisions with the electrons of the target's atoms, referred to as 'electronic', and elastic collisions, referred to as 'nuclear' where the atom as a whole recoils. The antimatter experiments at CERN rely on this phenomena to slow the 5.3 MeV antiproton beam delivered by the Antiproton Decelerator (AD) [1] to trappable energies. A combination of the high initial kinetic energy of the antiproton beam and limitations on the particle trapping voltages has meant that in typical cases less than 1% of the antiproton beam is trapped. The ASACUSA collaboration achieved a higher capture efficiency by employing an additional RF decelerating cavity at the entrance to their experiment [2], at the expense of a device with added complexity, cost, and size.

ELENA is a new ring which will decelerate the antiproton beams from the AD to 100 keV [3]. The reduced initial kinetic energy of the beam will increase the percentage of trappable antiprotons by up to two orders of magnitude. To accommodate for ELENA, experiments need to upgrade their particle apparati. The following paper presents a portion of the proposed modifications for the ALPHA Experiment, but applicable to other Penning trap based experiments.

Particles exiting the ALPHA degrader enter into a Penning-Malmberg charged particle trap [4], termed the 'Catching Trap' (CT), as shown in Fig. 1. Such a trap uses a strong axial magnetic field $\boldsymbol{B_z}$ for radial confinement and an electrostatic well for axial confinement that is limited to a longitudinal energy depth of ~ 5 keV for practical reasons. The trap has 18 low voltage electrodes, and two high voltage (HV) electrodes, HVA and HVB, used for capturing incoming antiproton bunches [5]. Particles emerging from the foils with energy less than 5 keV are reflected by a potential barrier of -5 kV (this is HVB in Fig. 1). Before these reflected particles can return to the degrader, a -5 kV potential is switched onto HVA and the capturing process is completed. Trapped particles then undergo sympathetic cooling and manipulation with preloaded electrons, until they are cold and dense enough for antihydrogen formation. Once this occurs, they are extracted to the atom trap, where they form antihydrogen through recombination with cold positron plasmas [6].

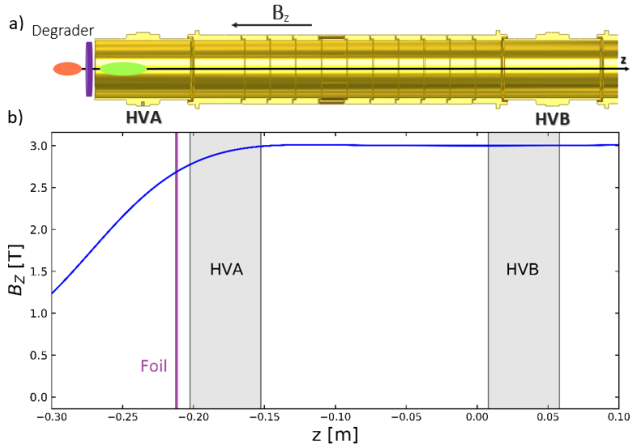

Figure 1: a) Partial schematic of the ALPHA degrader and catching trap electrodes (2012-2018). An example antiproton beam passes through the degrading foil from high energy (red) to low energy (green), and enters into the electrically-isolated cylindrical electrodes. HVA and HVB are special high voltage electrodes of inner diameter 29.6 mm. b) The longitudinal magnetic field $\boldsymbol{B_z}$ (blue) in the ALPHA catching trap, with $z = 0$ corresponding to its center.

We present an optimization study of the new degrading foil material, thickness, and location in the ALPHA CT for slowing future ELENA beams. A combination of analytic models, Monte Carlo simulation codes, and a particle tracking code have been employed to model the antiproton energy loss process and capture in the trap.

DEGRADING APPARATUS MATERIAL AND THICKNESS

The stopping power, $S(E)$, of a material is defined as the ion's mean energy loss per travelled path length, $-\mathrm{d}E/\mathrm{d}x$. Figure 2 displays the electronic stopping power for degrading materials considered in this study. We utilized two primary Monte Carlo simulation packages, SRIM-2013 [7] and

* siara.sandra.fabbri@cern.ch

ISBN: 978-3-95450-204-2 ISSN: 2673-5350 doi:10.18429/JACoW-IBIC2019-WEPP040

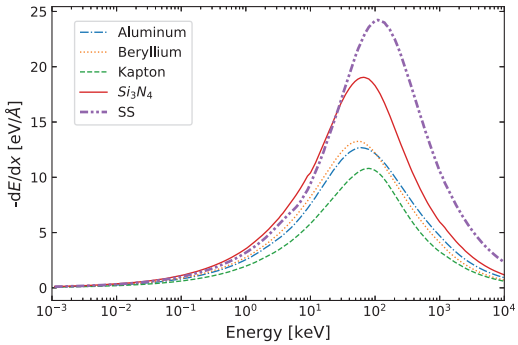

Figure 2: Electronic stopping powers for protons passing through various materials, as calculated by SRIM.

Geant4 [8], for modeling the energy loss process of ions transiting the degrader. Both packages use semiempirical models fit to experimental stopping power data, making them only as accurate as their data. A sparsity of experimental data below the stopping power maximum (see Fig. 2) has meant results are not expected to be accurate. SRIM is unable to simulate antiprotons, and although Geant4 does have this capability, results were invalid at low energies, leading us to simulate protons only. We preferentially adopted results from SRIM due to its reputation for being more accurate.

The design of the new degrading apparatus begins by determining the capture efficiency, η_c, for a range of suitable foil materials bombarded by 100 keV protons. η_c is defined here as the percentage of particles transmitted through the foil with $KE_z < 5$ keV. For all simulation results presented by SRIM and Geant4, the initial beam consists of 10^4 protons with zero initial divergence and momentum spread. Geant4 simulations use a step size of 0.01 µm, and the reference physics list QGSP_BIC_EMY [9]. Figure 3 displays the total percentage of particles transmitted as well as the percentage transmitted with with $KE_z < 5$ keV, η_c, through the majority of materials considered.

The thickness at which the maximum capture efficiency occurs for each material deviates by no more than 50 nm as computed by the two simulation codes, while a more significant difference is observed between the amplitude of the peaks. As the location of the peak is more important than the absolute height, this is an encouraging result in practice. Picking aluminum as an example, an optimal thickness of 0.83–0.835 µm allows for capturing ~ 50–70% of 100 keV protons as calculated by SRIM and Geant4 respectively. Geant4 Kapton and carbon results are absent due to errors in the simulation code. Figure 4 displays the capture efficiency computed by SRIM for all materials together for comparison.

Based on these results, the new degrading apparatus will be on the order of 1 µm thick. This has multiple consequences for the experimental configuration. First, the foil cannot act as a sealed vacuum window, making ALPHA's vacuum open to ELENA. Second, the extreme fragility of a 1 µm foil mandates extra care and precautions. The foil will be monolithic so as to have the greatest possible structural integrity.

The longitudinal and transverse energy distributions of the particles exiting the foil must also be considered. A material which creates small longitudinal and transverse energy spreads is desirable to minimize particle loss after the foil. Figure 5 displays the particle energy distributions after the optimal thickness of each material as calculated by SRIM. Materials with a higher concentration of particles in the longitudinal energy range below 5 keV, such as beryllium and kapton, have the highest capture efficiency. These materials also have the narrowest transverse energy spreads, making them the ideal choice.

The final decision of the new foil material depends not only on the optimal capture efficiency and particle energy distributions after the foil, but also on engineering considerations such as current manufacturing capabilities, structural integrity, and thermal conductivity. The properties of alu-

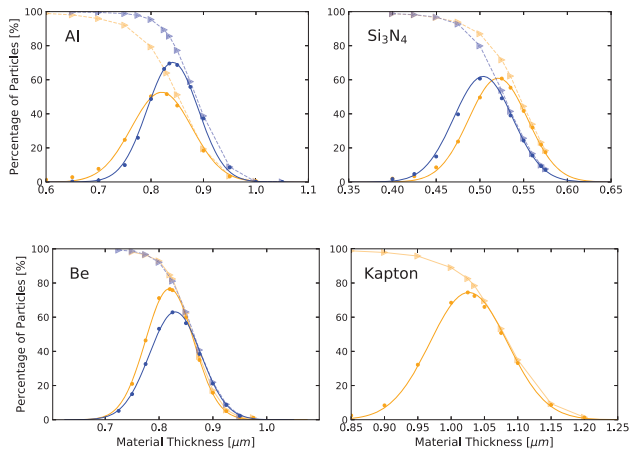

Figure 3: Geant4 (blue) and SRIM (orange) simulation results for: the total percentage of incident particles transmitted through the foil (dashed curves with triangles); the percentage of incident particles transmitted with $KE_z < 5$ keV, η_c (solid curves with dots).

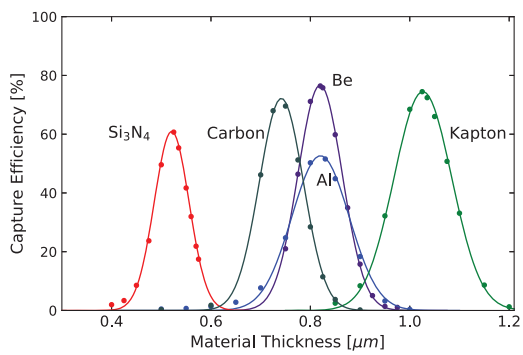

Figure 4: SRIM simulation results for the capture efficiency of: Si_3N_4 (red), carbon (grey), aluminum (blue), beryllium (purple), and Kapton (green).

ISBN: 978-3-95450-204-2 ISSN: 2673-5350 doi:10.18429/JACoW-IBIC2019-WEPP040

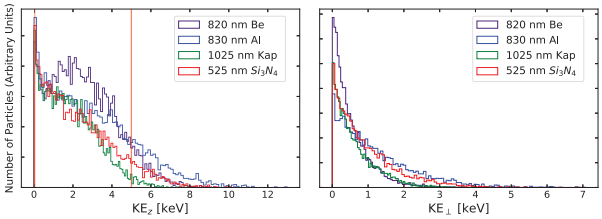

Figure 5: SRIM simulation results for the longitudinal and perpendicular energy spreads of particles exiting a material at its optimal thickness. Those particles with $KE_z < 5$ keV are highlighted by vertical red lines. The $KE_\perp$ distributions include only trappable particles, 40 eV $< KE_z <$ 5 keV.

minum and availability at 1 μm thicknesses make it the best candidate for this application and simulations going forward focus on this material.

The optimal foil thickness results must be modified to be applicable to antiprotons. Below ~ 2 MeV, negatively charged particles experience a smaller stopping power due to the Barkas Effect [10]. Stopping power data for antiprotons exists for a limited amount of materials at these low energies [11]. Figure 6 displays the stopping power for protons and antiprotons in aluminum.

By integrating the SRIM proton stopping power curve from 100 keV to 5 keV and the antiproton interpolated curve from 100 keV to 5 keV, the thickness of aluminum required to slow the relevant particles down can be determined. With this method, we found that antiprotons penetrate approximately 73.25% more material due to the Barkas Effect. Applying this to the optimal thickness of aluminium determined for protons by SRIM, 830 nm, the optimal thickness for antiprotons becomes 1438 nm. This assumes a straight-line trajectory approximation, which becomes unrealistic at

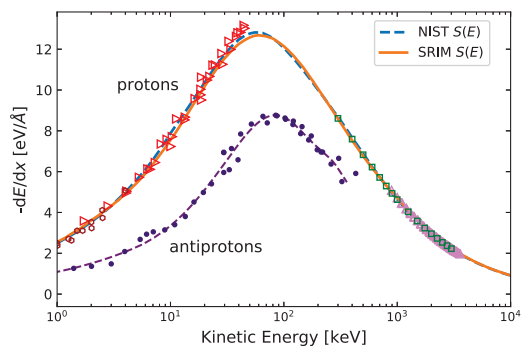

Figure 6: Electronic stopping power $S(E)$ for protons and antiprotons in aluminum. Data points for protons are: red and purple triangles, green squares, and brown circles, from refs. [12, 13, 14, 15] respectively. Fitted stopping power curves for protons are from SRIM (orange) and the NIST database (blue dashed) [16]. Antiproton data points are purple dots, from Ref. [11], and have a fitted curve (purple dashed).

low energies and makes this computed foil thickness likely an overestimation.

In a recently developed molecular dynamics simulation for modeling antiprotons slowing in matter [17], the authors determined the optimal aluminum foil thickness for an ELENA beam trapped by 5 kV potentials to be 910 ± 30 nm [18]. Although this model includes realistic antiproton trajectories and a modified nuclear stopping power for antiprotons, it seems to overestimate the electronic stopping power measured in [11]. For this reason, we will test a range of foil thicknesses between our computed optimal thickness and the optimal thickness in [18].

PARTICLE LOSS AFTER THE FOIL

All particles which transmit through the foil in SRIM are directly tracked into the ALPHA CT using the particle tracking simulation code GPT [19]. The initial energy distributions of the particle input beam for GPT are derived from the SRIM 830 nm aluminum foil simulation, while the spatial and temporal distributions are generated to match incident ELENA beam parameters based on the assumption that a 1 μm foil does not significantly change these. Space charge is ignored in the simulations presented. Figure 7 displays the GPT input beam spot size and temporal length.

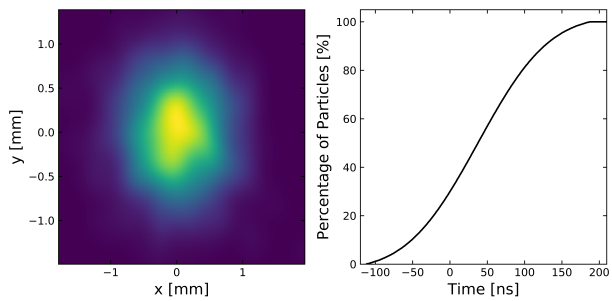

Figure 7: The initial spatial (left) and temporal (right) distributions of the particle input beam in GPT. These correspond to ELENA beam parameters: a 1 mm gaussian spot size beam that is 75 ns long.

Particles emerging from the degrading foil can be lost for several reasons after the foil. One such particle loss mechanism is the magnetic mirror effect [20]. It is described by the adiabatic invariant $\mu = mv_\perp^2/2|\boldsymbol{B}|$, where $v_\perp$ is the ion's velocity component perpendicular to $\boldsymbol{B}$. From conservation of energy, a particle adiabatically transiting from B_i to B_f and mirroring is characterised by,

$$\frac{\boldsymbol{v}_{\perp i}^2}{B_i} = \frac{\boldsymbol{v}_i^2}{B_f}, \quad (1)$$

where $\boldsymbol{v}_{\perp i}$ is the initial transverse velocity and v_i the total initial velocity. Equation (1) can be used to solve the final longitudinal magnetic field value, B_f, a particle can reach before reflecting. If B_f exceeds the maximum magnetic field value in z in the ALPHA catching trap (3 T) the particle will

ISBN: 978-3-95450-204-2 ISSN: 2673-5350 doi:10.18429/JACoW-IBIC2019-WEPP040

not mirror and is either trappable or lost through HVB. Using this approach, the percentage of transmitted particles (see Fig. 3) which are trappable (defined here as η_T), mirrored (defined here as η_M), or are lost through HVB (defined here as η_{HVB}) was found as a function of the aluminum foil location, shown in Fig. 8.

To avoid the significant effects of mirroring, it is evident that the foil should sit as close to HVA as possible. In this location, only ~ 0.5% of particles with $KE_z < 5$ keV mirror. If mechanical constraints necessitated the foil to sit further from HVA, a scenario of biasing the foil to some potential to accelerate antiprotons through the magnetic field gradient and into the trap was explored. However, only upwards of 10% of antiprotons could be recovered.

As the particles emerge and cyclotron orbit out of the foil, they have some chance of radially clipping into the foil mount or HVA. The number of particles lost as a function of the foil mount length and inner diameter directly guides the mechanical design of the mount. A simulation of an ELENA beam exiting a SRIM 830 nm aluminum foil, passing through an example mount geometry, and entering HVA is shown in Fig. 9. A range of realistic foil mount inner diameters for on and off axis beams were studied. The final mount ID decided upon was 14 mm, with 3.5 % of particles being lost over the 12 mm distance to HVA.

Not only must the radial size of the beam fit within the trap but so must its longitudinal size. As the beam emerges from the foil, its length will increase due to the large longitudinal energy spread induced by degrading, as shown in Fig. 5. Trappable particles within will reflect off of HVB and travel back towards HVA at which point HVA will turn on to complete the capturing process. If HVA is turned on too early or too late, most of the beam will have been either cut off or lost upstream respectively. By scanning over the time at which HVA turns on, a maximum in the percentage of trappable particles can be found as shown in Fig. 10

The left plot in Fig. 10 displays the density distribution of the beam as particles either reflect back towards HVA or

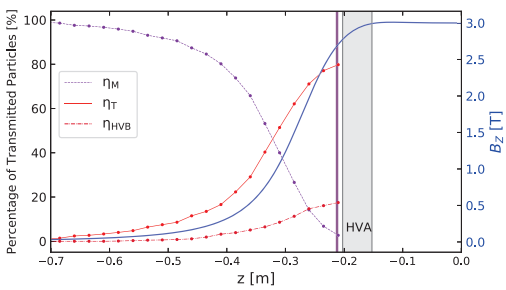

Figure 8: The percentage of transmitted particles which can be trapped, (η_T, red curve with red dots) or are either lost to mirroring (η_M, purple curve with purple dots) or escape through HVB (η_{HVB}, dashed maroon curve with maroon dots), as a function of the initial foil location. $z = 0$ corresponds to the center of the solenoidal magnetic field, B_z (solid blue curve), shown for reference.

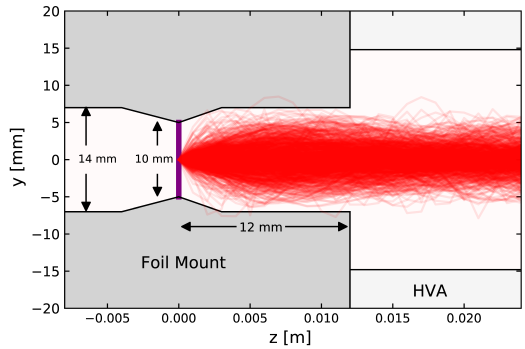

Figure 9: The trajectories of an ELENA beam (red) exiting a SRIM 830 nm aluminum foil (purple), located at $z = 0$, passing through an example foil mount geometry, and entering HVA. Only one transverse coordinate, y, is shown. Particle tracks stop when $v_z = 0$.

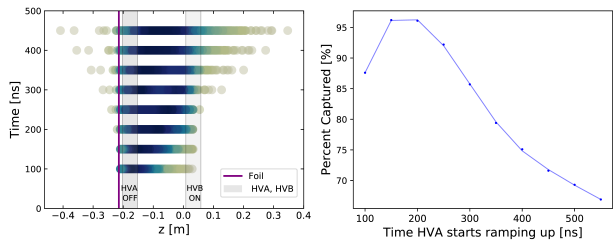

Figure 10: Left: time evolution of the longitudinal density distribution of the beam as particles either reflect from HVB back towards HVA or escape through HVB. Dark blue indicates the greatest density of particles. Right: the maximum in the percentage of trappable particles, η_T, which can be captured as a function of the time HVA ramps on. $t = 0$ corresponds to the time at which the ELENA beam strikes the foil.

escape through HVB. HVA is at zero voltage so that leftward escaping particles as a function of time can be seen. From the right plot in Fig. 10, the optimal ramp up time is ~ 200 ns, with only 3.8% of the trappable particles being lost.

Further explorations into particle loss in more exotic geometries is ongoing. A rotated foil can change the thickness of material the beam experiences, thereby tuning the degrading efficiency. Quantitative results are still being produced, however from initial inspection, a significant percentage of particles would be lost.

CONCLUSION AND OUTLOOK

The new ALPHA degrading apparatus for slowing down future 100 keV antiprotons from the ELENA storage ring has been designed. A monolithic, aluminum foil of thickness between 910 nm to 1438 nm will allow for catching upwards of roughly 50% of the incoming antiproton beam from ELENA. Detailed investigations into factors which limit the lifetime of the foil, such as pressure differentials and heating sources, are ongoing.

ISBN: 978-3-95450-204-2 ISSN: 2673-5350 doi:10.18429/JACoW-IBIC2019-WEPP040

REFERENCES

[1] S. Maury, "The antiproton decelerator (ad)," *Hyperfine Interactions*, vol. 109, pp. 43–52, 1997.

[2] N. Kuroda *et al.*, "Development of a monoenergetic ultraslow antiproton beam source for high-precision investigation," *Phys. Rev. ST Accel. Beams*, vol. 15, p. 024702, 2012.

[3] T. Eriksson *et al.*, "The elena project: Progress in the design," in *Proc. IPAC'12,* New Orleans, LA, USA, May 2012, paper THPPP008, pp. 3740–3742.

[4] G. Gabrielse *et al.*, "Open-endcap penning traps for high precision experiments," *Int. J. Mass Spectrom.*, vol. 88, pp. 319–332, 1989.

[5] C. Amole *et al.*, "The alpha antihydrogen trapping apparatus," *Nucl. Inst. Meth.*, vol. 735, pp. 319–340, 2014.

[6] M. Ahmadi *et al.*, "Observation of the 1s-2s transition in trapped antihydrogen," *Nature*, vol. 541, p. 506, 2017.

[7] J. F. Ziegler *et al.*, "Srim–the stopping and range of ions in matter (2010)," vol. 268, pp. 1818–1823, 2010.

[8] S. Agostinelli *et al.*, "Geant4—a simulation toolkit," vol. 506, pp. 250–303, 2003.

[9] A. Ribon *et al.*, "Status of geant4 hadronic physics for the simulation of lhc experiments at the start of lhc physics program," tech. rep., CERN, 2010.

[10] A. H. Sørensen, "Barkas effect at low velocities," *Nucl. Inst. Meth.*, vol. 48, pp. 10–13, 1990.

[11] S. Møller *et al.*, "Direct measurements of the stopping power for antiprotons of light and heavy targets," *Phys. Rev. A*, vol. 56, p. 2930, 1997.

[12] S. Møller *et al.*, "Antiproton stopping at low energies: Confirmation of velocity-proportional stopping power," *Phys. Rev. Lett.*, vol. 88, p. 193201, 2002.

[13] M. Moro *et al.*, "Traceable stopping cross sections of al and mo elemental targets for 0.9–3.6-mev protons," *Phys. Rev. A*, vol. 93, p. 022704, 2016.

[14] H. Bichsel, "Shell corrections in stopping powers," *Phys. Rev. A*, vol. 65, p. 052709, 2002.

[15] D. Primetzhofer *et al.*, "Electronic excitations of slow ions in a free electron gas metal: evidence for charge exchange effects," *Phys. Rev. Lett.*, vol. 107, p. 163201, 2011.

[16] M. J. Berger *et al.*, *Stopping-power and range tables for electrons, protons, and helium ions*. Gaithersburg, MD, USA: NIST Physics Laboratory, 1998.

[17] K. Nordlund *et al.*, "Nuclear stopping power of antiprotons," *Phys. Rev. A*, vol. 96, p. 042717, 2017.

[18] K. Nordlund, "Slowing down of 100 kev antiprotons in al foils," *Results in Physics*, vol. 8, pp. 683–685, 2018.

[19] M. De Loos and S. Van der Geer, "General particle tracer: A new 3d code for accelerator and beamline design," in *Proc. EPAC'96,* Sitges, Spain, Jun. 1996, paper THP001G, pp. 1245 – 1247.

[20] M. Galand and A. D. Richmond, "Magnetic mirroring in an incident proton beam," *J. Geophys. Res. Space Phys.*, vol. 104, pp. 4447–4455, 1999.